Effect of Rigid Particle Size on the Toughness of Filled Polypropylene

I. L. Dubnikova, S. M. Berezina, A. V. Antonov

N. N. Semenov Institute of Chemical Physics, RAS, 4 Kosygin St., Moscow 119991 Russia

Received 29 July 2003; accepted 24 March 2004
DOI 10.1002/app.21017
Published online in Wiley InterScience (www.interscience.wiley.com).

ABSTRACT: The role of rigid particle size in the deformation and fracture behavior of filled semicrystalline polymer was investigated with systems based on polypropylene (PP) and model rigid fillers [glass beads, $Al(OH)_3$]. The regularities of the influence of particle content and size on the microdeformation mechanisms and fracture toughness of the composites at low and high loading rates were found. The existence of the optimal particle size for fixed filler content promoting both maximum ultimate elongation of the composite at the tensile and maximum toughness at impact test was shown. The decrease of the toughening effect with both decreasing and increasing particle size regarding the optimal one was explained by dual role of particle size, correspondingly as either "adhesive" or "geometric" factors of fracture. The adhesive factor is due by the increase of debonding stress with the particle size decrease and the voiding difficulty resulting in the restriction of plastic flow. The geometric factor consists in the dramatic decrease of the composite strength at break if the void size exceeds the critical size of defect (for a given matrix) at which the crack initiation occurs. The analysis of the filled polymer toughness dependencies upon the particle size revealed that a capacity of rigid particles for the energy dissipation at the high loading rate depends on two factors: (i) ability of the dispersed particles to detach from matrix and to initiate the matrix local shear yielding at the vicinity of the voids and (ii) the size of the voids forming. Based on the findings it was concluded that the optimal minimal rigid particle size for the polymer toughening should answer the two main requirements: (i) to be smaller than the size of defect dangerous for polymer fracture and (ii) to have low debonding stress (essentially lower compared to the polymer matrix yield stress). © 2004 Wiley Periodicals, Inc. J Appl Polym Sci 94: 1917–1926, 2004

Key words: poly(propylene) (PP); composites; fillers; particle size; mechanical properties; impact resistance; toughness

INTRODUCTION

At the heart of the mechanism for rubber toughening is relief of hydrostatic tension during polymer deformation by the cavitation of rubber inclusions followed by local shear yielding of the matrix polymer surrounding voids.[1–5] The effectiveness of energy dissipation at the high loading rate is connected to ability of the elastomer to create voids.[6,7] The polymer fracture toughness increases with increasing rubber phase content and decreasing elastomer inclusion size.[8] The transition from brittle to ductile fracture of blends occurs at critical rubber particle content or size.[9–13] One of existent criteria of brittle–ductile transition is a decrease in an interparticle distance to fixed critical (for a given matrix) polymer ligament thickness.[9–13] The rise in the toughening efficiency with decreasing elastomer particle size is supposed to be a result of more intense decrease of ligament thickness with the rubber fraction increase.

Correspondence to: I. L. Dubnikova (ild@chph.ras.ru).

Journal of Applied Polymer Science, Vol. 94, 1917–1926 (2004)

However the rubber modification is accompanied by a dramatic loss in stiffness. A new concept is the use of rigid filler as a toughening agent. The data available on the influence of the rigid inclusions on the plastic properties of semicrystalline polymers and on the fracture process are ambiguous. Most of the studies report an embrittling effect on polymers and a significant loss of toughness compared to the neat polymer.[14,15] At the same time there are a few cases that show an increase in impact resistance of polymers (HDPE, PP) upon addition of a rigid filler.[16–21] The possibility of rigid particles to polymer toughening originates from the debonding at the particle–polymer interface and micropores nucleating followed by shear yielding of the surrounding matrix polymer.[18–21] A significant influence of the interface adhesion and particle size on the toughening efficiency of rigid particles was observed in these cases.[16–24] The results presented by Vollenberg et al.[25] and Zhuk et al.[26] reveal that the particle size is the parameter influencing the debonding stress of inclusions (σ_d) during loading of filled polymers. With the decrease in particle size, the σ_d increases[26] and the voiding intensity decreases.[27–29]

The purpose of this work was to understand the role of rigid particle size in the fracture of filled polymers.

TABLE I
The Ranges of Filler Particle Size

Filler	Particle size (μm)		
	Average	Minimum	Maximum
GB	0.2		
	3.5	1	10
$Al(OH)_3$	1	0.5	2
	3	1.5	5
	8	4	16
	25	5	50
	55	17	80

The systems based on PP with different rigid particle contents and sizes were investigated. Glass beads and $Al(OH)_3$ were used as model rigid fillers with narrow size distributions. The regularities of the influence of particle size on the microdeformation mechanisms and fracture toughness of the composites at impact conditions and tensile test were compared.

EXPERIMENTAL

Materials

Isotactic PP (Moscow Naphta Processing Plant. Ltd., Russia) with a melt flow rate (MFR) = 0.38 g/10 min (190°C, 5 kg) was used as a matrix polymer ($M_w = 6.3 \times 10^5$ g/mol, $M_w/M_n = 3.5$). The narrow fractions of aluminum hydroxide (Sumitomo Smelting Co. Ltd., Japan) and glass beads (GB) (Potters-Ballotini 5000 CP-03) were used as rigid fillers. The ranges of particle sizes are shown in Table I.

Compounding

Composites were prepared by melt blending the components in a mixing chamber (Brabender mixing chamber, 190°C, 60 rpm, 10 min) in the presence of calcium stearate (2 wt % with respect to filler). Thermal stabilizers topanol (0.3 wt %) and dilauriltiodipropionate (0.5 wt %) were used. The neat PP was processed in similar way.

Specimen preparation

The specimens for mechanical testing were prepared by compression molding. The molding procedure involves heating at 190°C for 5 min without applied pressure and then for 5 min under pressure (10 MPa). The mold was cooled to 90°C by water at the rate of 16°C/min under pressure.

Tensile test

Dumbbell-shaped specimens were cut from a 0.5-mm-thick molded sheet. Tensile properties of samples were measured at ambient temperature using a tensile testing machine Instron-1122 with a crosshead speed of 20 mm/min (0.67 min^{-1}). The average values were calculated from eight runs for each sample.

Impact tests

The impact strength of notched specimens was measured at ambient temperature by notched Izod and three-point bending tests. Izod impact tests were carried out at 2.9 m/s on rectangular bars 80 × 10 × 4 mm with a single-edge 45° V-shaped notch (tip radius 0.25 mm, depth 1.5 mm). Three-point bending tests were carried out at 2.6 m/s on rectangular bars 40 × 6 x 4 mm also with a single-edge 45° V-shaped notch (tip radius 0.25 mm, depth 1.5 mm). All of tests were performed at ambient temperature. The average values were calculated from seven runs for each sample.

Scanning electron microscopy (SEM)

The particle distribution in initial undeformed composite was examined by SEM analysis of cryogenically fractured surfaces using the JEOL JSM-35C. The microdeformation processes and failure modes were studied by analysis of the tensile deformed film surfaces and the fracture surfaces of impact fractured specimens. All specimens were gold-sputtered before SEM analysis.

RESULTS AND DISCUSSION

Tensile test

Effect of particle size on the composition dependencies of ultimate elongation of the filled PP

Neat PP deforms with necking followed by strain hardening. The influence of rigid particle volume

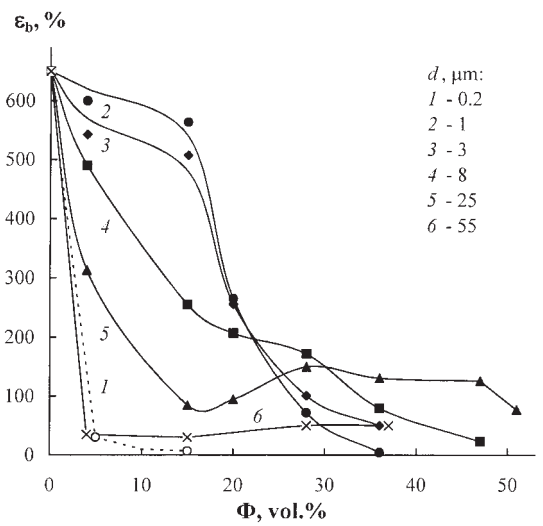

Figure 1 The composition dependencies of ε_b for composites with different particle size.

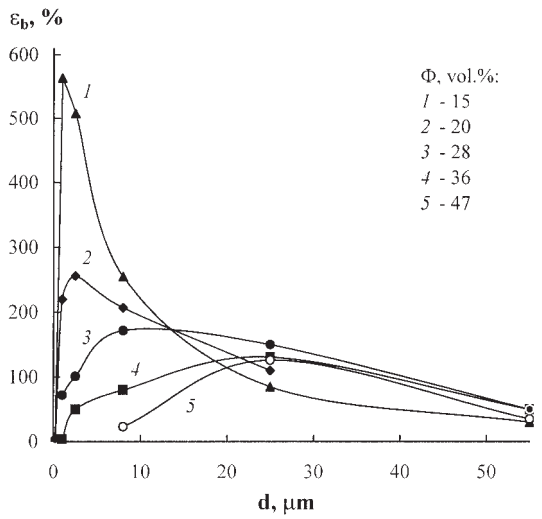

Figure 2 The dependencies of ε_b upon particle size for different regions of Φ.

content (Φ) and size ($\bar{d}$) on an ultimate elongation (ε_b) of the filled PP is demonstrated in Figure 1. The $\bar{d}$ range is from 0.2 to 55 μm. As seen, a character of composition dependency of ε_b–Φ depends substantially on the inclusion size and filler content. Figure 2 shows the dependencies of ε_b upon $\bar{d}$ for various filler content. They have extreme character and at any Φ the optimal particle size ($\bar{d}_{opt}$) exists that favors a maximum ability of the filled polymer to plastic deformation. The $\bar{d}_{opt}$ value increases with filler content increasing. A similar effect was shown in our previous papers for particulate-filled HDPE.[28–30]

In the area of $\Phi \leq 20$ vol % the optimal particle size is 1–3 μm. The composites with $\bar{d}_{opt}$ show the stable neck propagation and strain hardening like neat PP (Fig. 3, curves 2–4). In such composites a smooth decrease of the ε_b with Φ and ductile fracture are observed (Fig. 1, curve 2). The smaller ($\bar{d}$ = 0.2 μm) and larger ($\bar{d}$ = 8–55 μm) particles reduce sharply the ability of filled polymers to plastic deformation and composites fracture at low ε_b [Fig. 4(a)]. In the range of $\Phi > 20$ vol % the composites containing particles of 1 and 3 μm undergo the transition from ductile to brittle fracture [Fig. 1, curves 2 and 3; Fig. 4(b), curve 1]. In this Φ range the composites with $\bar{d}_{opt}$ = 25 μm have the highest ε_b [Fig. 4(b), curve 2]. The large plastic deformations are due to a change of plastic flow mechanism from a macroinhomogeneous with necking to a macrohomogeneous one into numerous craze-like zones (Figs. 1 and 3, curve 5).

Dual role of particle size in the processes of plastic flow and fracture: As either adhesive or geometric factor

The drop of ε_b with both decreasing and increasing particle size regarding $\bar{d}_{opt}$ was explained by the character of particle debonding microprocesses, namely, by dual role of particle size in the fracture behavior of filled polymer: as either "adhesive" or "geometric" factors.

The adhesive factor originates from that with the decrease in $\bar{d}$ the σ_d increases[26] and the debonding intensity tends to reduction.[27] The interfacial exfoliation events and pore nucleating during loading can be detected from the σ–ε diagram as the decrease in the stress of the onset of inelastic deformation (the elastic limit σ_e) compared to one of neat PP (Table II).[25,30,31] If particle debonding takes place on the early stage of loading (low σ_d) most inclusions debond from matrix before macroscopic yielding. In this case the filled polymer yield stress $\sigma_y(\Phi)$

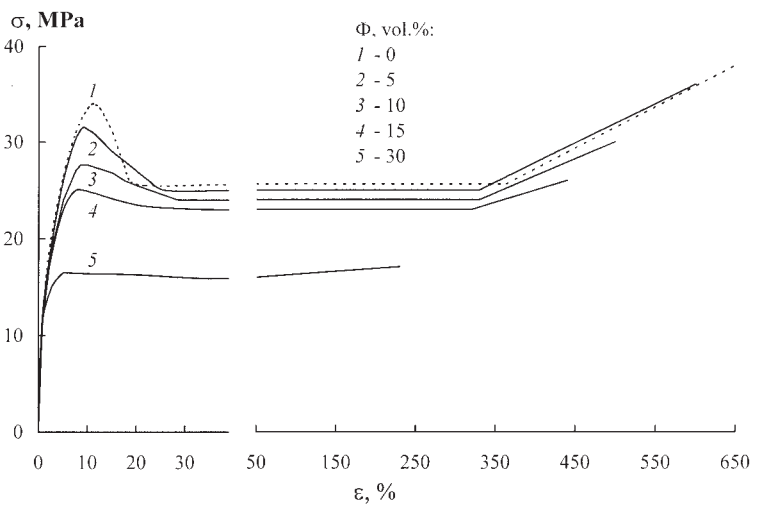

Figure 3 Stress–strain diagrams for the composites with $\bar{d}_{opt}$ depending on Φ. The $\bar{d}_{opt}$ values are 1 μm (curves 2–4) and 25 μm (curve 5).

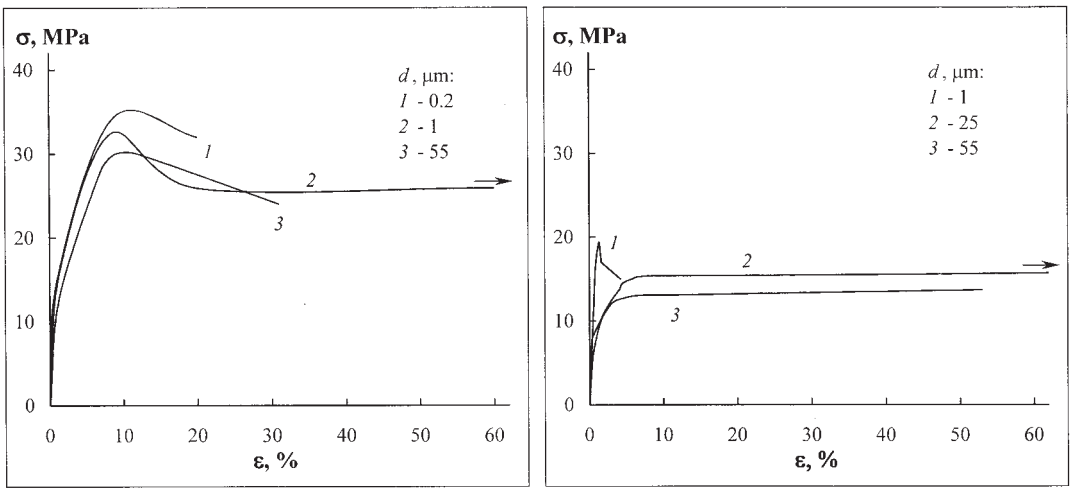

Figure 4 Stress–strain diagrams for the composites with $\bar{d} < \bar{d}_{opt}$ (curves 1) and $\bar{d} > \bar{d}_{opt}$ (curves 3) at $\Phi = 5$ vol % (a) and $\Phi = 36$ vol % (b).

is described well by a base dependence for composite with zero adhesion $\sigma_y = \sigma_y^m(1 - \Phi^{2/3})$ (σ_y^m is the matrix yield stress)[32] and the σ_y decreases with Φ as a result of the decrease in an effective load-bearing section with the void content increase. The condition of debonding most particles before yielding is[27]

$$\sigma_d < \sigma_y^m(1 - \phi^{2/3}) \quad (1)$$

The low σ_e and an accordance of the σ_y–Φ dependence to base one are typical for composites with large particles (Table II).

Since the σ_y of composite with fully debonded particles decreases with Φ, while the σ_d does not change practically with filler content, for fixed particle size (fixed σ_d) some critical filler content $\Phi = \Phi_{cr}$ should exist at that the condition

$$\sigma_d \geq \sigma_y^m(1 - \phi^{2/3}) \quad (2)$$

will be realized and the transition from complete debonding to the incomplete one and the decrease in a portion of debonded inclusions will occur.[27] An influence of the σ_d on the transition to incomplete debonding signifies the role of particle size as adhesive factor. At incomplete debonding the composite yield stress is higher compared to that for composite with fully debonded inclusions and close to corresponding σ_d.[27,31,33] As seen from Table II, the σ_y values of composites containing small particles with increasing Φ become higher corresponding values for composites with large inclusions. For particles of 0.2 μm the deflection of yield stress from the base dependence $\sigma_y(\Phi)$ occurs already at negligible filler content ($\Phi \approx 5$ vol %). It is mind that $\bar{d} =$ 0.2 μm is critical small particle size for that the σ_d is close to σ_y of PP matrix. According to data presented above, the regions of $\bar{d} < \bar{d}_{opt}$ (for the fixed Φ values) on the ε_b–$\bar{d}$ dependencies (Fig. 2) correspond to regions of the particle sizes where their role as an "adhesive factor" is realized. The drastic drop of composite ε_b in range $\bar{d} < \bar{d}_{opt}$ is due to the ductile–brittle transition as result of the preservation of high σ_y in combination with a decrease of tensile strength σ_b with the Φ (because of total particle debonding on the fracture stage) and realization of the condition

$$\sigma_b < \sigma_y \quad (3)$$

The relationship between the particle size and the character of microdeformation processes was studied by SEM analysis of deformed sample surfaces. Debonding most of particles during loading is observed in the composites with $\bar{d}_{opt}$. The SEM micrograph of the sample with 10 vol % particles of 1 μm taken from the neck shoulder area [Fig. 5(a)] reveals that at the initial stage voids initiate the formation of microporous deformation zones. When the deformation increases a transformation of such zones to neck occurs. On the strain hardening stage [Fig. 5(b)] the voids are distributed homogeneously and strongly elongated along stretching direction as a result of plastic deformation of the surrounding matrix. This suggests that, in the case of the $\bar{d}_{opt}$, pore formation does not hamper the drawing process and the composites fracture in ductile manner like unfilled PP (Fig. 3). At higher Φ in composites with $\bar{d}_{opt} = 25$ μm the plastic deformation develops within numerous microporous zones of craze-like

TABLE II
Effect of Filler Content and Particle Size on the Tensile Mecanical Properties of Composites

Filler	$\bar{d}$ (μm)	ϕ (vol %)	E (MPa)	σ_e (MPa)	σ_y (MPa)	ε_y (%)	σ_b (MPa)	ε_b (%)
—	—	0	1300	16.2	35.0	10.0	43.0	650
GB	0.2	5	1395	18.7	35.7	8.7	36.2	20
		10	1529	21.1	33.3	5.1	36.2	9
		15[a]	1895	17.4	—	—	29.9	7
GB	3.5	5	1400	15	31.2	9.0	36.0	600
		10	1540	14.4	27.4	8.2	30	500
		15	1800	13.8	24.8	7.0	26.0	440
		30	1950	13	16.8	5.6	17.1	230
$Al(OH)_3$	1	4	1490	16.1	32.5	8.5	35.0	580
		15	1700	15.8	25.8	4.5	30.7	564
		20	2000	16.0	25.0	2.8	23.7	200
		28	2350	16.0	22.9	2.2	19.6	72
		36	2520	16.1	19.4	1.3	16.7	4
$Al(OH)_3$	3	4	1470	15.8	32.1	8.3	36.0	543
		15	1700	15.9	25.3	7.3	29.8	508
		20	2020	16.3	22.3	4.9	24.4	256
		28	2210	16.2	20.2	3.1	19.8	101
		36	2260	15.6	16.6	1.2	15.0	50
$Al(OH)_3$	8	4	1400	16.0	32.0	8.3	32.5	490
		15	1760	16.0	25.5	5.8	25.2	255
		20	2000	16.1	24.0	5.6	23.8	207
		28	2130	15.1	18.0	4.8	17.6	172
		36	2230	14.1	15.5	4.2	15.5	80
		47	2160	13.8	12.0	1.4	11.4	23
$Al(OH)_3$	25	4	1430	14.9	31.0	6.7	29.1	313
		15	1670	11.6	25.0	6.6	23.2	85
		20	1800	9.1	22.4	7.0	22.8	95
		28	2040	8.2	17.2	6.8	17.7	150
		36	2170	7.6	15.4	6.8	16.2	131
		47	1670	6.6	11.0	7.0	11.8	126
$Al(OH)_3$	55	4	1360	12.9	30.0	8.5	23.0	31
		15	1660	9.0	24.3	6.8	22.5	30
		28	1617	5.1	16	—	16.3	50
		36	1747	4.7	13.6	—	13.8	50

[a] Quasi-brittle fracture.

type [Figs. 5(c) and (d)]. The macrohomogeneous character of plastic flow of this specimen (Fig. 3, curve 5) is the result of a high concentration of craze-like zones.

SEM micrographs of the surfaces of tensile deformed samples with $\bar{d} < \bar{d}_{opt}$ are demonstrated in Figure 6 for composites with 5 vol % particles of 0.2 μm [Figs. 6(a) and (b)] and for composites with 36 vol % particles of 1 μm [Fig. 6(c)]. It is seen that microprocesses of interfacial exfoliation are limited and most inclusions stay adhesive bonded with the matrix. The localized yielding and quasi-brittle fracture occurs within a restricted zone, outside one in which the particles are not debonded.

In the range of $\bar{d} > \bar{d}_{opt}$ particle-matrix debonding is observed at all ranges of Φ studied (Fig. 7). As debonding is a not limiting factor, the decrease of ultimate elongation of composites with large particles can be explained by a geometric factor, namely by the large size of voids formed. The role of the void size is due to an existence of critical defect size exceeding at which drastic decrease of composite tensile strength occurs. At low Φ the composites with large particles fracture after the yielding starts on the stage of neck propagation ($\bar{d}$) = 25 μm) [Fig. 7(a)] or neck formation ($\bar{d}$) = 55 μm) [Fig. 7(b)]. The physical nature of critical defect size is not clear at the present time and this parameter evidently characterizes the sensitivity of polymer to defect. SEM analysis of specimens with 5 vol % particles of 25 μm diameter, taken from the neck region, shows that the characteristic feature of plastic deformation in the presence of large particles is an evolution of diamond-shaped voids [Fig. 7(a)]. It was supposed that large pores make it difficult for the polymer matrix to draw out and hamper the strain hardening, in contrast to small voids ($\bar{d}_{opt}$) [Fig. 4(b)]. At higher Φ the composites with $\bar{d}$ (3) = 55 μm have the lowest values of elongation and tensile strength at break. Thus the loss of a capacity for the high plastic deformation with increasing $\bar{d} > \bar{d}_{opt}$ is due by the

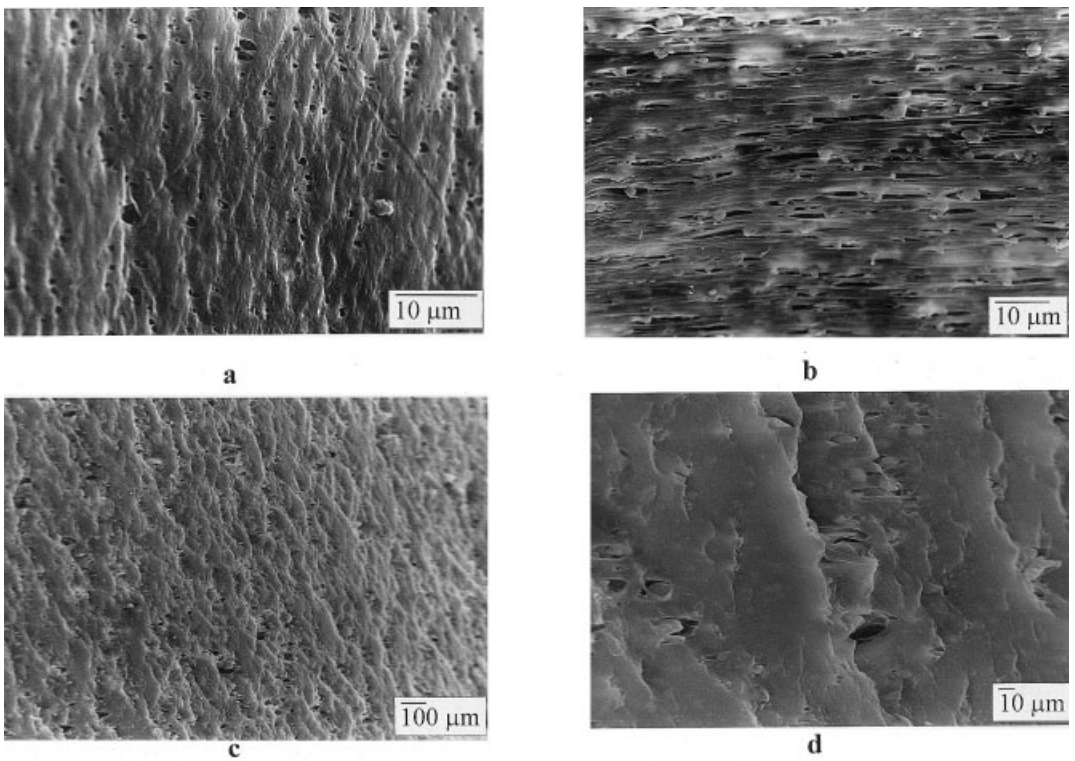

Figure 5 The SEM micrographs of surfaces of tensile deformed samples with $\bar{d}_{opt}$: (a and b) $\bar{d} = 1$ μm at $\Phi = 10$ vol %: (c and d) $\bar{d} = 25$ μm at $\Phi = 36$ vol %. (a) Microporous craze-like zones in neck shoulder area; (b) elongated voids in strain hardening region; (c) numerous microporous craze-like zones, where the plastic flow occurs during macrohomogeneous deformation; (d) isolated craze-like zones. The tensile direction is horizontal.

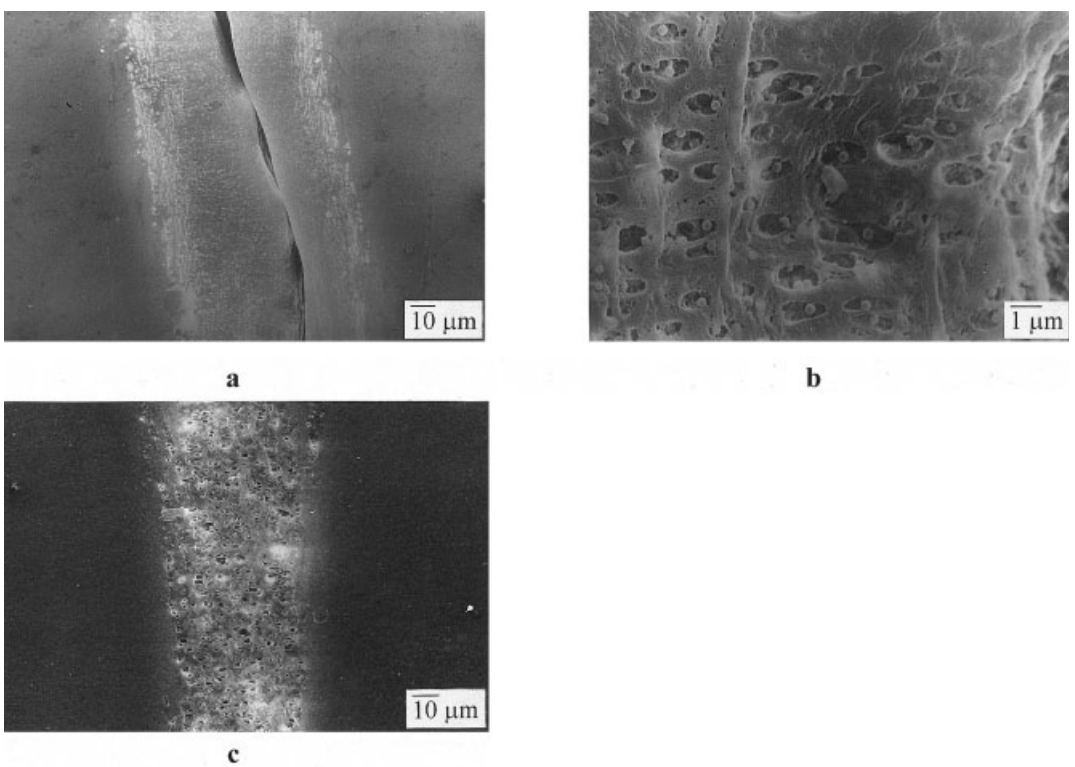

Figure 6 The SEM micrographs of surfaces of tensile deformed samples with $\bar{d} < \bar{d}_{opt}$: (a and b) $\bar{d} = 0.2$ μm at $\Phi = 5$ vol %; (c) $\bar{d} = 1$ μm at $\Phi = 36$ vol %. (a) The crack across localized plastic zone; (b) the debonding small particles within plastic zone; (c) localized plastic zone. The tensile direction is horizontal.

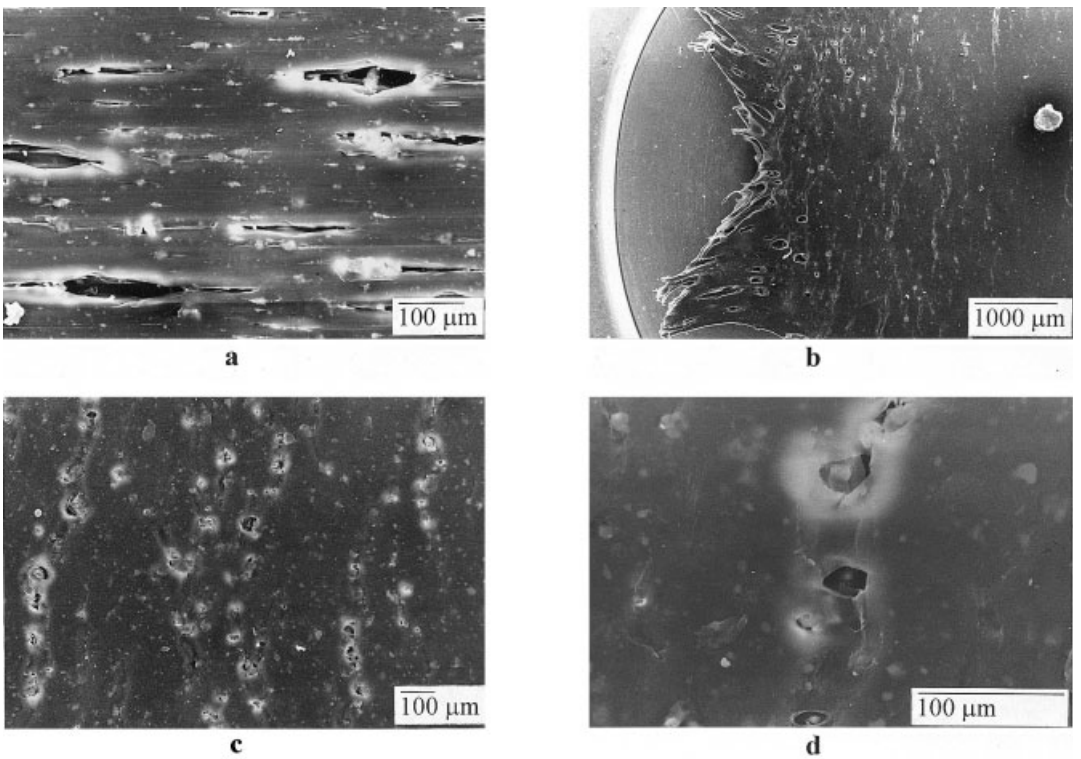

Figure 7 The SEM micrographs of surfaces of tensile deformed samples with $\bar{d} > \bar{d}_{opt}$: (a) $\bar{d}$ = 25 μm at Φ = 5 vol %; (b) $\bar{d}$ = 55 μm at Φ = 5 vol %; (c and d) $\bar{d}$ = 55 μm at Φ = 36 vol %. (a) Diamond-shaped voids on the neck propagation stage; (b) fracture from large defect on the initial stage of necking; (c) microporous craze-like zones; (d) initiation of crack in the vicinity of large defect. The tensile direction is horizontal.

realization of a condition[3] as a result of the drastic decrease of σ_b with the particle size increase.

Impact test

Effect of particle content and size on the toughness of the filled PP

At the impact loading the unfilled PP fractures in a brittle manner. The effect of rigid particle content and size on the relative notched Izod impact strength of filled PP ($A_{rel} = A/A^{PP}$) is reported in Figure 8. It appears that the particle size strongly affects the impact behavior of composites. The addition of a negligible amount of the smallest particles of 0.2 μm dramatically decreases the impact strength (curve 1). The introduction of the particles with $\bar{d}$ = 1 and 3 μm seems to result in the most significant improvement of the filled PP impact resistance (curves 2 and 3). In this case the dependencies of A_{rel}–Φ are extreme; the maximum A_{rel} value is reached about $\Phi \approx$ 10–15 vol % and right up to Φ = 30 vol % the composite toughness stays higher compared to that for neat PP. In this filling region the composites containing larger particles ($\bar{d}$ = 8 and 25 μm) show impact energies close to the value for neat PP (curves 4, 5). At $\Phi > 30$ vol % the inversion of the A_{rel}–Φ dependencies occurs: the impact strength of composite with $\bar{d}$ = 1 μm sharply drops (curve 2), whereas the composites with the particles of 8 and 25 μm keep the larger impact resistance (curves 4, 5).

Figure 9 illustrates the dependencies of A_{rel} upon $\bar{d}$ for various filler contents. They are extreme and for

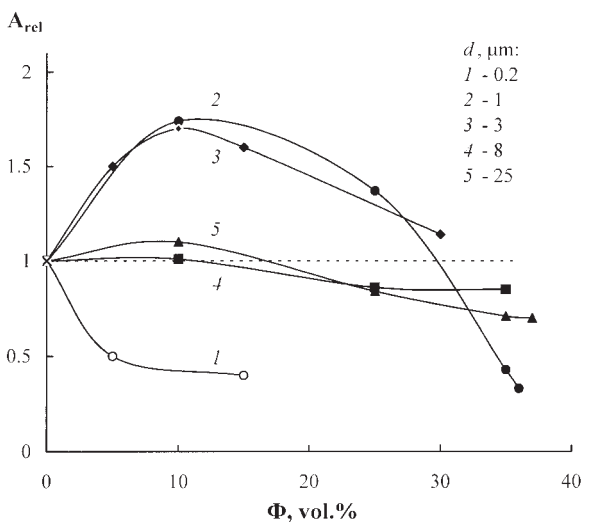

Figure 8 The composition dependencies of the relative notched Izod impact strength of filled PP with different particle sizes.

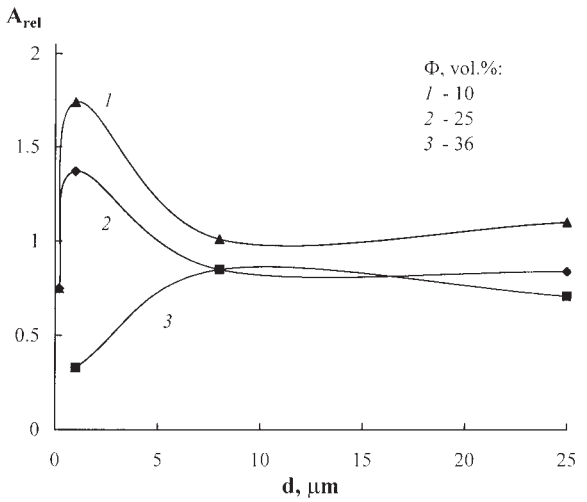

Figure 9 The dependencies of A_{rel} upon particle size for different Φ.

fixed Φ the optimal particle size $\bar{d}_{opt}$ exists where the maximum improvement of the composite notched Izod impact strength is achieved. At filler content lower then 30 vol % the $\bar{d}_{opt}$ value is 1–3 μm, and at Φ higher than 30 vol % one shifts to larger $\bar{d}$. It appears that the regularities of the influence of particle size on the matrix ability to plastic deformation are similar for the low and high loading rates.

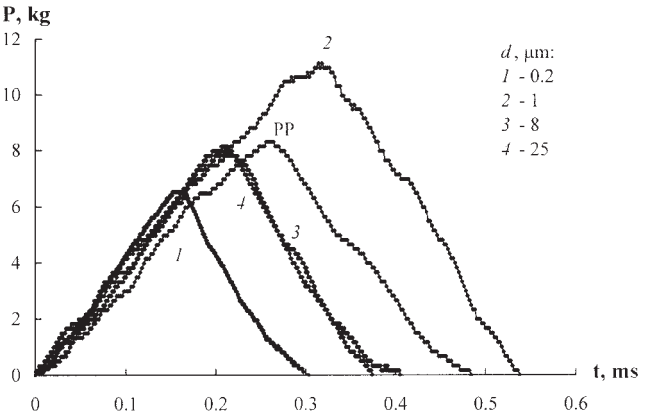

Figure 11 The load-time diagrams for the neat PP and composites with different particle sizes at Φ = 10 vol %.

Fracture micromechanisms

Figures 10 and 12 illustrate the morphologies of the impact fracture surfaces of composite specimens with different particle sizes for Φ = 10 and 36 vol % and Figures 11 and 13 are the load-time diagrams of the composites corresponding. In the composite containing particles of 0.2 μm diameter [Fig. 10(a)] crack propagation is not accompanied by debonding inclusions and the composite fractures cohesively in a brittle manner. In contrast in the composites with larger

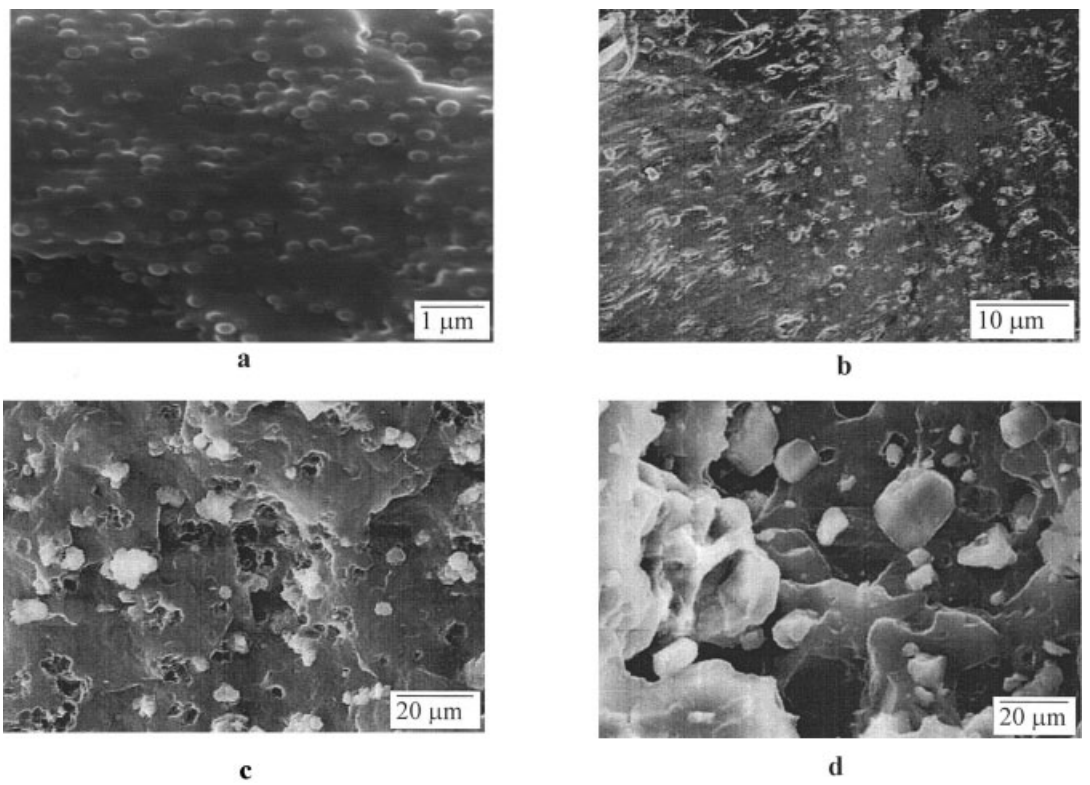

Figure 10 SEM fractographs of impact fractured specimens with 10 vol % particles of 0.2 (a), 1 (b), 8 (c), and 25 (d) μm. The taking area is near the notch. The direction of crack propagation is from left to right.

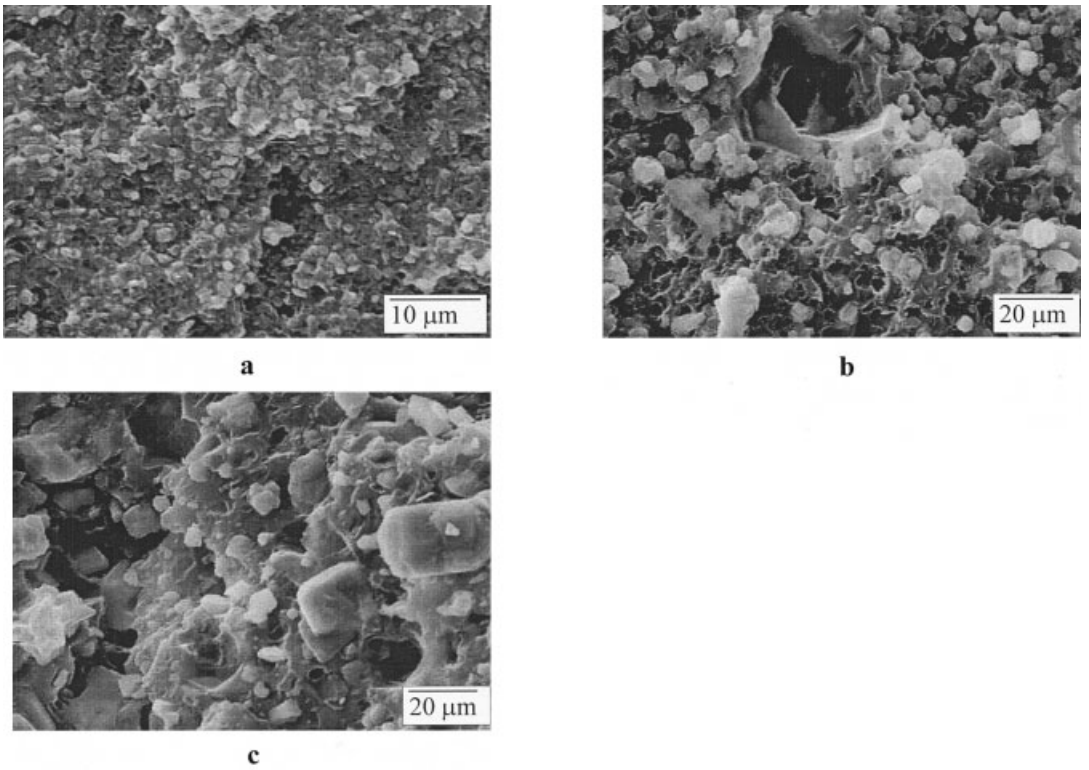

Figure 12 SEM fractographs of impact fractured specimens with 36 vol % particles of 1 (a), 8 (b), and 25 (c) μm. The taking area is near the notch. The direction of crack propagation is from left to right.

particles the debonding inclusions and voiding are observed [Figs. 10(b)–(d)]. A distinguishing feature of the fracture plane of composite containing particles with $\bar{d}_{opt} = 1$ μm is the presence of strongly elongated voids near the notch [Fig. 10(b)]. Evidently, particle debonding and the small size of void formed cause the extensive yielding of the surrounding matrix during loading. Load–time diagrams confirm that the significant improvement of the notched Izod impact strength of composite with $\bar{d} = 1$ μm is due to larger plastic deformation on the initial stage of crack initiation preceding fracture (Fig. 11).

In the range $\Phi > 30$ vol % an embrittleness of the composite with $\bar{d} = 1$ μm occurs and fracture energy decreases compared to that of neat PP (Fig. 8). As appears from the fractograph [Fig. 12(a)] at this Φ the inclusions of 1 μm stay bonded with the matrix during crack propagation and the transition from adhesive to cohesive fracture occurs. In the systems with larger inclusions the particle debonding and adhesive character of the composite fracture are observed [Fig. 12(b) and (c)]. Load–time diagrams of the composites with $\Phi = 36$ vol % reveal that the result of difficulty voiding in the composite with $\bar{d} = 1$ μm is the significant limitation of the plastic deformation on the crack initiation stage and more brittle fracture of the material (Fig. 13).

Thus it appears that the regularities of the influence of particle size on the microdeformation processes and matrix ability to plastic deformation are similar for the low and high loading rates.

CONCLUSION

The analysis of the effect of the particle size on the filled polymer toughness revealed that the capacity of rigid particles for energy dissipation at high loading rates depends on two factors: (i) ability of the dispersed particles to detach from matrix (low debonding stress) and to initiate the matrix local shear yielding at

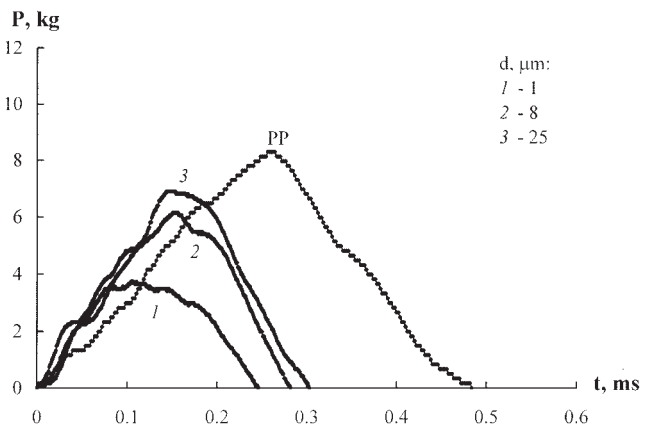

Figure 13 The load–time diagrams for the neat PP and composites with different particle sizes at $\Phi = 36$ vol %.

the inclusion–polymer interface and (ii) the size of void formation. The existence of an optimal particle size promoting maximum plastic properties of the composite at fixed filler content was found for both low and high loading rates. The decrease of the toughening effect with decreasing particle size regarding $\bar{d}_{opt}$ was explained by the role of particle size as the adhesive factor of fracture. The adhesive factor is due to the increase of debonding stress with the particle size decrease and the incomplete particle debonding. The difficulty of voiding leads to a composite brittle fracture as the result of the high yield stress and the restriction of plastic flow. The decrease of the toughening effect with increasing particle size regarding $\bar{d}_{opt}$ was explained by the role of particle size as the geometric factor of fracture. It consists in the dramatic decrease of the composite strength at break if the void size exceeds the size of a critical defect at which the crack initiation occurs.

Based on the findings it was concluded that the optimal minimal rigid particle size for the polymer toughening should meet two main requirements: (i) to be smaller than the size of defect dangerous for polymer fracture and (ii) to have low debonding stress. The last condition means that the debonding stress of particles with $\bar{d}_{opt}$ should be essentially lower compared to the polymer matrix yield stress.

The authors thank the Russian Foundation of Fundamental Research, Project No.01–03-32,043, for financial support of this work.

References

1. Bucknell, C. B. Toughened Plastics; Applied Science Publishers: London, 1977.
2. Chiu, C. J., Vijayan, K., Kirby, D., Hiltner, A., Baer, E. J Mater Sci 1988, 23, 2521.
3. Dijkstra, K.; Ter Laak, J.; Gaymans, R. J. Polymer 1994, 35, 315.
4. Lazzeri, A. L.; Bucknall, C. B. Polymer 1995, 36, 2895.
5. Jiang, W.; Yuan, Q.; An, L.; Jiang, B. Polymer 2002, 43, 1555.
6. Borggreve, R. J. M.; Gaymans, R. J.; Schuijer, J. Polymer 1989, 30, 71.
7. Borggreve, R. J. M.; Gaymans, R. J.; Eichenwald, H. M. Polymer 1989, 30, 78.
8. Orazio, L. D.; Mancarella, C.; Martuscelli, E.; Polato, F. Polymer 1991, 32, 1186.
9. Wu, S. Polymer 1985, 26, 1855.
10. Wu, S. J Appl Polym Sci 1988, 35, 549.
11. Muratoglu, O. K.; Argon, A. S.; Cohen, R. E., Weinberg, M. Polymer 1995, 36, 4771.
12. Muratoglu, O. K.; Argon, A. S.; Cohen, R. E.; Weinberg, M. Polymer 1995, 36, 4787.
13. Bartczak, Z.; Argon, A. S.; Cohen, R.E.; Weinberg M. Polymer 1999, 40, 2331.
14. Liang, J.–Z. J Appl Polym Sci 2002, 83, 1547.
15. Fridrich, K.; Karsch, U. A. Fibre Sci Technol 1983, 18, 37.
16. Fu, Q.; Wang, G.; Shen, J. J Appl Polym Sci 1993, 49, 673.
17. Fu, Q.; Wang, G. J Appl Polym Sci 1985 1993, 49.
18. Bartczak, Z.; Argon, A. S.; Cohen, R. E.; Weinberg, M. Polymer 1999, 40, 2347.
19. Liu, Z. H.; Kwok, K. W.; Li, R. K. Y.; Choy, C. L. Polymer 2002, 43, 2501.
20. Thio, Y. S.; Argon, A. S.; Cohen, R. E.; Weinberg, M. Polymer 2002, 43, 3661.
21. Zuiderduin, W. C. J.; Westzaan, C.; Huetink, J.; Gaymans, R J. Polymer 2003, 44, 261.
22. Pukanszky, B.; Voros, G. Compos Interfaces 1993, 1, 411.
23. Dongming, L. I.; Wenge, Z.; Zongneng, O. I. J Mater Sci 1994, 29, 3754.
24. Mai, K.; Li, Z.; Qiu, Y.; Zeng, H. J Appl Polym Sci 2002, 84, 110.
25. Vollenberg, P.; Heikens, D.; Ladan, H. C. B. Polym Compos 1988, 9, 382.
26. Zhuk, A.V.; Knunyantz, N. N.; Topolkaraev, V. A.; Oshmian, V. G.; Berlin, A. A. J Mater Sci 1993, 28, 4595.
27. Dubnikova, I. L.; Oshmian, V. G.; Polym Sci Ser A 1998, 40, 925.
28. Topolkaraev, V. A.; Tovmasyan, Y. M.; Dubnikova, I. L.; Petrosyan, A. I.; Meshkova, I. N.; Berlin, A. A.; Enikolopyan, N. S. Dokladi Acad Nauk SSSR 1986, 290C, 1418.
29. Topolkaraev, V. A.; Tovmasyan, Y. M.; Dubnikova, I. L.; Petrosyan, A. I.; Meshkova, I. N.; Berlin, A. A.; Gomza, Y. P.; Shilov, V. V. Mekhanica Kompoz Mater 1987, 616.
30. Dubnikova, I. L.; Oshmian, V. G.; Gorenberg, A.Y. J Mater Sci 1997, 32, 1613.
31. Dubnikova, I. L.; Berezina, S. M.; Antonov, A. V. J Appl Polym Sci 1911 2002, 85.
32. Nicolais, L.; Narkis, M. Polym Eng Sci 1971, 11, 194.
33. Dubnikova, I. L.; Berezina, S. M.; Oshmian, V. G.; Kuleznev, V. N. Polym Sci Ser A 2003, 45, 873.